Research, Society and Development, v. 10, n. 12, e310101220362, 2021
(CC BY 4.0) | ISSN 2525-3409 | DOI: http://dx.doi.org/10.33448/rsd-v10i12.20362

Modelling and simulation of the ion exchange process for Zn^{2+}(aq) removal using zeolite NaY

Modelagem e simulação do processo de troca iônica para remoção de Zn^{2+}(aq) usando zeólita NaY

Modelado y simulación del proceso de intercambio iónico para la eliminación de Zn^{2+}(aq) utilizando zeolita NaY

Received: 09/08/2021 | Reviewed: 09/16/2021 | Accept: 09/20/2021| Published: 09/23/2021

Andrezza de Araújo Silva Gallindo
ORCID: https://orcid.org/0000-0001-7288-2311
Federal University of Campina Grande, Brazil
E-mail: andrezza.araujo@eq.ufcg.edu.br
Reinaldo Alves da Silva Junior
ORCID: https://orcid.org/0000-0002-9593-3021
Federal University of Pernambuco, Brazil
E-mail: reinaldo.alves@ufpe.br
Meiry Gláucia Freire Rodrigues
ORCID: https://orcid.org/0000-0003-2258-4230
Federal University of Campina Grande, Brazil
E-mail: meiry.rodrigues@ufcg.edu.br
Wagner Brandão Ramos
ORCID: https://orcid.org/0000-0002-9375-6995
Federal University of Campina Grande, Brazil
E-mail: wagner.ramos@eq.ufcg.edu.br

Abstract
The treatment of water contaminated by toxic metals using ion exchange with zeolites is becoming attractive due to its low capital costs and high potential for removal capacity. Mathematical modelling of this process allows for operational control and estimation of the ability to remove these metals. In this work, the kinetic modelling was performed based on finite bath experimental data, with Intraparticle Diffusion (IPD) and External Liquid Film Mass Transfer (MTEF) models. The models Thomas (TH), Yoon-Nelson (YN) and Solid Film Mass Transfer (MTSF) were used to estimate the saturation time, ion exchange capacity and sizing variables of a fixed bed column. For the finite bath system, the results showed that the mass transfer was better represented by the IPD phenomenon. The breakthrough curve obtained by the Aspen Adsorption (MTSF) model presented the best fit, compared with experimental data, with $R^2 \geq 0.9923$. The average ion exchange capacities calculated for MTSF, TH and YN were respectively 2.22, 2.12 and 2.07 meq Zn^{2+}(aq)/ g of zeolite. The model simulated with Aspen Adsorption was also used to analyze the continuous system behaviour, by varying the height of the bed. It was observed that increasing the height, the saturation time and ion exchange capacity also increase, while reducing the height makes axial dispersion the predominant mass transfer phenomenon, which reduces the diffusion of Zn^{2+}(aq) ions.
Keywords: Ion exchange; NaY zeolite; Aspen Adsorption; Simulation; Kinetic modelling.

Resumo
O tratamento de águas contaminadas por metais tóxicos por meio da troca iônica com zeólitas vêm se tornando atrativo pelo baixo custo de capital e alto potencial de remoção. A modelagem matemática desse processo permite o controle operacional e a estimativa da capacidade de remoção desses metais. Neste trabalho, a modelagem cinética foi realizada sob dados experimentais de banho finito, com modelos de Difusão Intrapartícula (IPD) e Transferência de Massa em Filme Líquido Externo (MTEF). Os modelos Thomas (TH), Yoon-Nelson (YN) e Transferência de Massa em Filme Sólido (MTSF) foram usados para estimar o tempo de saturação, a capacidade de troca iônica e variáveis de dimensionamento de uma coluna de leito fixo. No sistema de banho finito, os resultados mostraram que a transferência de massa foi melhor representada pelo fenômeno IPD. A curva de breakthrough obtida pelo modelo Aspen Adsorption (MTSF) apresentou o melhor ajuste, em comparação com os dados experimentais, com $R^2 \geq 0{,}9923$. As capacidades médias de troca iônica calculadas para MTSF, TH e YN foram respectivamente 2,22, 2,12 e 2,07 meq Zn^{2+}(aq)/g de zeólita. O modelo simulado com Aspen Adsorption também foi utilizado para analisar o comportamento do sistema contínuo, variando a altura do leito. Observou-se que aumentando a altura, o tempo de saturação e a capacidade de troca iônica também aumentam, enquanto a redução da altura torna a dispersão axial o fenômeno de transferência de massa predominante, o que reduz a difusão dos íons Zn^{2+}(aq).
Palavras-chave: Troca iônica; Zeólita NaY; Aspen Adsorption; Simulação; Modelagem cinética.

Resumen
El tratamiento de agua contaminada por metales tóxicos mediante intercambio iónico con zeolitas es atractivo debido a su bajo costo de capital y alto potencial de remoción. El modelado de procesos matemáticos permite el control operativo y la estimación de la capacidad de remoción de metales. En este trabajo, el modelado cinético se realizó bajo datos experimentales de baño finito, con modelos de Difusión Intrapartícula(IPD) y Transferencia de Masa de Película Líquida Externa(MTEF). Se utilizaron los modelos Thomas(TH), Yoon-Nelson(YN) y Solid Film Mass Transfer(MTSF) para estimar el tiempo de saturación, la capacidad de intercambio iónico y las variables de tamaño de la columna de lecho fijo. En el sistema de baño finito, los resultados definieron la transferencia de masa mejor representada por el fenómeno DPI. La curva de avance obtenida por el modelo Aspen Adsorption(MTSF) presentó un mejor ajuste a los datos experimentales, con $R^2 \geq 0{,}9923$. Las capacidades medias de intercambio iónico calculadas para MTSF, TH e YN fueron respectivamente 2,22, 2,12 y 2,07 meq Zn^{2+}(aq)/ g de zeolita. El modelo simulado en Aspen Adsorption también se utilizó para analizar el comportamiento del sistema continuo, variando la altura del lecho. Se observó que el aumento de altura, el tiempo de saturación y la capacidad de intercambio iónico también aumentan, mientras que la reducción de altura hace que la dispersión axial sea el fenómeno predominante de transferencia de masa, reduciendo la difusión iónica de Zn^{2+}(aq).
Palabras clave: Intercambio iónico; Zeolita NaY; Aspen Adsorption; Simulación; Modelado cinético.

1. Introduction

Heavy metals are still causing environmental problems in the 21st century, such as the pollution of rivers connected to public water sources, due to unstructured urbanization and industrial processes (Oliveira et al., 2018).

According to the 2019 Statistical Yearbook of the Metallurgical Sector, the Brazilian production of zinc was in 2nd place among non-ferrous metals. This intense production process results in high waste disposal. The National Council for the Environment, through resolution CONAMA 430/2011 of Brazil, establishes that the maximum concentration for disposal of zinc in the receiving body is 5 mg/L. The EPA (United States Environmental Protection Agency) recommends the National Secondary Drinking Water Regulations (NSDWRs) 5 mg/L of Zinc. Based on Cupertino et al. (2020) zinc has nutritional importance, however in high doses it presents toxicity and health risks. Zinc oxide nanoparticles, for example, present in battery, biomedical and food production industries, are related to the decrease in cellular antioxidant levels (Lazzaretti & Hupffer, 2018).

Most effluent and water purification processes containing excess of toxic metals, which employ ion exchange technology, use fixed bed columns. To model this dynamic process, it is interesting to know the chemical balance, kinetics and mass balances of the system (Nakajima, 2013). For fixed bed modelling, the Thomas (TH) and Yoon – Nelson (YN) models are considered useful by some authors (Zheng et al., 2008; Trgo et al., 2011) however, according to Abdi and Abedini (2020), Aspen Adsorption software models have also been efficient.

The Aspen Adsorption (Adsim) software is a tool used to simulate dynamic adsorption and ion exchange processes, which provides models for the generation of breakthrough curves and estimation of performance parameters for continuous fixed bed. The Adsim model was used in recent researches, such as simulation of the ion exchange of Cu2+ in aqueous solution with the biomass Cucumis melo VAR. cantalupensis, (Nieva et al., 2018), Cu(II) and Cr(III) on charcoal (Zhang et al., 2019) and Cd (II) and Cu (II) in simple and binary metallic systems with the biomass Eichhornia crassipes (Adornado et al., 2016).

1.1 Objectives

In this work, an investigation was carried out regarding possible kinetic modelling using finite bath experimental data from literature (Intraparticle Diffusion and External Film Mass Transfer models). Fixed bed column models (MTSF, TH and YN) were obtained to represent the removal of Zn2+(aq) in aqueous medium, by ion exchange, with zeolite NaY. The model obtained with Aspen Adsorption (MTSF) was used to evaluate the influence of the bed height on the Zn2+(aq) ion removal capacity by the zeolite NaY, in a continuous fixed bed column.

2. Methodology

This research was carried out in four distinct steps: (1) bibliographic research of significant experimental data on the removal of $Zn^{2+}_{(aq)}$ by NaY zeolite in finite bath and fixed bed column; (2) kinetic modelling of finite bath data using the Intraparticle Diffusion (IPD) and External Film Mass Transfer (MTEF) models to determine the limiting step for the mass transfer (TM); (3) kinetic modelling of fixed bed column data using the models: Solid Film Mass Transfer (MTSF) from Aspen Adsorption, Thomas (TH) and Yoon-Nelson (YN), to compare the significance of each and identify mass transfer and axial dispersion phenomena involved in the process; (4) simulation of the ion exchange process between $Zn^{2+}_{(aq)}$ and NaY zeolite.

2.1 Sources of Experimental Data

Table 1 presents the list of experimental data extracted from Ostroski et al. (2008) which were necessary for the adjustments of the IPD, MTEF, MTSF, TH and YN kinetic models explored in this research.

Calculations of some other parameters were performed to satisfy specifications of the Aspen Adsorption model (MTSF). To this end, data referring to the physical characteristics of zeolite NaY were collected from Silva and Souza (2004) and are presented in Table 2. These data were used to calculate interparticle and intraparticle voids (ε_i and ε_p).

Table 1. Experimental data on $Zn^{2+}_{(aq)}$ removal by NaY zeolite.

Data	Value	Description	Method
q_m	2.83 ± 0.14 meq.g^{-1}	Langmuir constants	Finite bath
b	3.06 ± 0.61 meq.g^{-1}		
C_0	0.586 to 2.447 meq.L^{-1}	Feeding concentration	Fixed Bed Column
Q	8 mL.min^{-1}	Feed flow	
D_b	0.009 m	Column diameter	
H_b	0.03 m	Useful height of the column	
ε_i	0.5	Column porosity	
Dp	0.18 mm	Particle diameter	

Source: Ostroski (2008).

Column porosity (ε_i), referring to the volume of voids in the fixed bed column, was determined by Equation (1), based on Silva and Souza (2004).

$$\varepsilon_i = 1 - \left(\frac{\rho_{ulk}}{\rho_{true}}\right) \quad (1)$$

Table 2. Experimental parameters for the characterization of NaY zeolite.

Value	Description	Method
0.8959 kg.m^{-3}	Bulk Density	Mercury porosimetry
0.54	Porosity	
3,03.10-4 m^3.kg^{-1}	Total pore volume	Helium Gas Picnometry
1.9807 Kg.m^{-3}	True Density	

Source: Silva and Souza (2004)

Applying data from Table 2 to Equation (1), it was possible to calculate ε_i = 0.54 m^3/m^3, a value close to ε_i = 0.5, found by Ostroski et al. (2008), presented in Table 1. Due to the convergence of ε_i values, the characterization data in Table 2

were also considered to calculate the particle porosity (ε_p), referring to the total pore volume of a material (V_{pore}), using Equation (2), based on Silva and Miranda (2003).

$$\varepsilon_p = \frac{V_{pore}}{1/\rho_{true} + V_{pore}} \quad (2)$$

The calculated ε_p value was 5.99×10^{-4} m^3/m^3. Another variable calculated to satisfy the software model was the selectivity constant (K_{AB}), using Equation (3) based on Abrão (2014) where the distribution coefficient q_0 is the total number of meq of the cation in the exchanger per gram of resin, and C_0 is the total ion concentration, in meq per mL of solution.

$$K_A^B = K_d \frac{C_0}{q_0} \quad (3)$$

The selectivity constant (K_{AB}) belongs to the ion exchange equilibrium governed by the Law of Mass Action, which was used, in Aspen Adsorption, to estimate the molar fraction of exchanged ions equivalent to the aqueous phase and the ion exchange bed, through Equation (4).

$$IP_{1A}\left(\frac{y_A}{xA}\right)\left(\frac{x_B}{yB}\right)^{IP_{2A}}\left(\frac{Q}{C_0}\right)^{IP_{2A}-1} = 1.0 \quad (4)$$

In Equation (4), the parameter IP1 is equal to K_{AB} and the parameter IP2 is the stoichiometric coefficient of the ion exchange reaction; *x* represents the equivalent molar fraction, in the ion exchange resin, of the ion (component A) and counter ion (component B); *y* represents the equivalent molar fraction in the aqueous phase of the ion (component A) and counter ion (component B); C_0 is the total ionic concentration ($eq.m^{-3}$) and Q represents the maximum volumetric ion exchange capacity of the resin ($eq.m^{-3}$).

The parameter K_d was calculated by fitting the models (Equations (5) to (8)) to the equilibrium data of the exchange between $Zn^{2+}_{(aq)}$ and Zeolite NaY obtained from Ostroski et al. (2008) The linear isotherm model is described by Equation (5) (Calábria et al., 2017). Lambert (1967) suggested a polynomial function of the equilibrium concentration presented in Equation (6). The linearized Langmuir isotherm is given by Equation (7) and the linearized Freundlich model is given by Equation (8) (Calvet, 1989):

$$q_e = K_d C_e \quad \text{or} \quad y = Bx \quad (5)$$

$$q_e = K_1 C_e + K_2 C_e^2 \quad \text{or} \quad y = Bx + Cx^2 \quad (6)$$

$$\frac{1}{q_e} = \frac{1}{q_m b C_e} + \frac{1}{b} \quad \text{or} \quad y = Bx + A \quad (7)$$

$$ln(q_e) = \ln(K_f) + (1/n) ln(C_e) \quad \text{or} \quad y = A + Bx \quad (8)$$

Where q_e (or *y*) is the amount of solute adsorbed by an amount of adsorbent, in equilibrium with a solution of concentration C_e (or *x*); K_d (or *B*) is the distribution coefficient of the solute between the solution and the solid surface; K_1 and K_2 (or *B* and *C*) are constant, and K_1 is the estimate of K_d of the product; q_m and *b* are constant and $q_m b$ (or *1/B*) is the

estimated K_d of the product; K_f (or $exp[A]$) is the Freundlich constant, $1/n$ is an index of the adsorption intensity and since $1/n$ = 1, $K_f = K_d$ is considered (Souza et al., 2001).

To determine the most suitable model for predicting the constant K_d, the following statistical criteria were evaluated: coefficient of determination (R^2) obtained by Equation (9) where SS_{res} is the residual sum of squares and SS_{tot} is the total sum of squares, the Mean Squared Error (MSE) obtained by Equation (10) where n is the data points on all variables, Y is the vector of observed values of the variable being predicted with $\hat{Y}$ being the predicted values, and the Standardized Residual Scatter Plot in which it is desirable that the residuals are in the range between -2 and +2, as well as well distributed along the zero mean, without presenting clusters of points (Montgomery & Peck, 1982).

$$R^2 = 1 - \frac{SS_{res}}{SS_{tot}} \tag{9}$$

$$MSE = \frac{1}{n}\sum_{i=1}^{n}\left(Y_i - \hat{Y}\right)^2 \tag{10}$$

2.2 Kinetic Modelling of Finite Bath

Adsorption kinetics studies demonstrate beneficial information about control mechanisms of adsorption processes, such as surface adsorption, chemical reaction and diffusion mechanisms (Montgomery & Peck, 1982). In this work, two kinetic models of mass transfer (IPD and MTEF) were fitted to the experimental data of the finite bath kinetics of ion exchange between $Zn^{2+}_{(aq)}$ and NaY zeolite, from Ostroski et al. (2008) to define which phenomenon represented the limiting step of the process.

2.2.1 Kinetic equation of Intraparticle Diffusion (IPD)

First and second order kinetic models are not able to determine the diffusion mechanism. For this purpose, it is preferable to evaluate the kinetic results with the intraparticle diffusion model, which is represented by Equation (11) in its linearized form (Abdi et al., 2017):

$$q_t = K_p t^{1/2} + I \tag{11}$$

Where q_t is the amount of solute in the solid phase at time t (meq/g); K_p is the intraparticle diffusion rate constant (meq/g/min$^{-0.5}$); I is the intercept.

2.2.2 Kinetic model of External Film Mass Transfer (MTEF)

The External Film Mass Transfer model assumes that the solute is removed from the solution until equilibrium is reached in the liquid film formed on the solid surface, and that the equilibrium concentration varies with time (Puranik et al., 1999). The total mass balance of the finite bath system and the convective model that described the mass transfer between the solution and the adjacent film was described according to Equation (12), adapted from Puranik et al. (1999).

$$\frac{dq}{dt} = \frac{V \cdot K_{tm}}{m} \cdot \left[C_0 - \frac{m \cdot q(t)}{V} - \frac{q(t)}{q_m \cdot b - q(t)} \right] \quad (12)$$

Where C is the concentration of adsorbate in solution (meq.L-1); K_{tm} is the liquid phase mass transfer coefficient (min^{-1}); t is time (min); q_m is the maximum equilibrium adsorption capacity; b is the Langmuir equilibrium isotherm constant; $q(t)$ is the amount of solute in the film adjacent to the surface at time t (meq/g); C_0 is the initial solution concentration ($meq.L^{-1}$); V is solution volume (L); m is the mass of adsorbent (g). The differential Equation (12) was solved numerically, using the 'ode45' routine from the MATLAB software and the experimental values of each parameter, obtained from Ostroski et al. (2008).

2.3 Modelling of Breakthrough Curves

For modelling the fixed bed column, the TH, YN and the MTSF Adsim models were fitted to the Breakthrough Curves presented by Ostroski et al. (2008) in order to verify the significance of the MTSF model in relation to other dynamic models also adjustable to this process.

2.3.1 Thomas Model (TH)

One of the most used models for predicting the breakthrough curve and evaluating the performance of a fixed bed column was proposed by Thomas (1944), expressed in Equation (13).

$$\frac{C}{C_0} = \frac{1}{1 + \exp[\frac{K_{TH}.q.m}{Q} - K_{TH}.C_0.t]} \quad (13)$$

Where q is the maximum solute concentration in the solid phase (meq/g); Q is the flow rate (mL/min); m is the exchanger mass (zeolite NaY) (g), C_0 is the feed concentration (meq/L); C is the output concentration; t is the time and K_{TH} is the Thomas model constant (mL/min.meq).

2.3.2 Yoon-Nelson Model (YN)

The Yoon-Nelson theoretical model has the characteristic of not requiring detailed information on the exchange process in the fixed bed column and still providing the process variable τ, which is the time required to reach the effluent concentration at 50% of the feed concentration (min), as well as calculate K_{YN}, the Yoon–Nelson constant (min^{-1}) (Jung et al., 2017). The fractional removal, C/C_0, is represented by Equation (14).

$$\frac{C}{C_0} = \frac{C_0.\exp[K_{YN}.(t-\tau)]}{1 + \exp[K_{YN}.(t - \tau)].C_0} \quad (14)$$

2.3.3 Aspen Adsorption (MTSF) Solid Film Ion Exchange Mass Transfer Model

In Aspen Adsorption software, the process modelling was governed by a set of differential equations that configure the ion exchange between the ion to be removed from the effluent and the exchangeable cation of the zeolite NaY. The ionic species $Zn^{2+}_{(aq)}$ in the liquid phase, fed into the ion exchange column, was governed by the MTSF model, represented by Equation (15), of mass balance and axially dispersed 'plug flow' moment (Tantet et al., 1994). The convection with estimated dispersion (Ez) was included in the mass balance through Equations (15) and (16) (Slater, 1991; Ruthven, 1984):

$$-\varepsilon_i E_z \frac{\partial^2 c_k}{\partial z^2} + v_l \frac{\partial c_k}{\partial z} + \varepsilon_i \frac{\partial c_k}{\partial t} + \varepsilon_p MTC_{SK}(W_k^* - W_k) = 0 \quad (15)$$

$$\frac{v_l d_p}{E_z} = 0.2 + 0.011 \left(\frac{Re}{\varepsilon_i}\right)^{0.48} \quad (16)$$

Where c_k is the ion concentration in the liquid phase (eq/m^3); E_z is the Axial dispersion coefficient (m^2/s); t is time (s); Z is the Axial Coordinate Axis; ε_i is bed void (porosity); MTC_{sk} is the solid film mass transfer coefficient (1/s); w_k is the resin ion loading (eq/m3); W_k* is the ion charge in equilibrium with the ion concentration in the liquid phase (eq/m3); v_l is the liquid velocity (m/s); d_p is the diameter of particles (m); Re is Reynolds number.

2.4 Process Simulation

The Aspen Adsorption software and MTSF model were also used to design new continuous systems by varying the column height, to assess what interference would occur under the saturation time and the ion exchange capacity.

Bed heights were based on the mass (m_b) of NaY zeolite used in the bed ion exchange study, as shown in Equation (17) (Nieva et al., 2019):

$$m_b = \frac{1}{4}\pi D^2 H_b \rho_b \quad (17)$$

Where D is the column diameter (m); H_b is the bed height (m) and ρ_b the bulk density of the exchanger (g). The choice of useful heights was established according to those that generated well-structured breakthrough curves, with a column saturation time different from zero (t[min]) and greater capacities for removing zinc from contaminated aqueous medium (q[meq/ g]). The flowchart shown in Figure 1, represents the entire simulation process carried out in this research.

The simulation was performed in transient regime with a time span of 1 second. The bed length was divided into 20 knots. The UDS1 was used as a discretization method and the system of discretized equations was integrated by the implicit Euler method with a variable step from 0.01 to 0.05. Furthermore, the thermodynamic model ELECNRTL (Electrolyte Non-Random Two Liquid) was used for the interaction of ions and water molecules and the parameters adjusted by the mass action law were used to estimate the equilibrium concentrations.

Assuming that the system has no interference with any obstruction, but only dissociation in pure water, the properties of $Zn^{2+}_{(aq)}$ were determined using Aspen Properties Electrolytes Wizard. To add the counterion from the ion exchange process, the component list was saved and converted to a component set. Based on the characterization of zeolite NaY performed by Ostroski et al. (2008) its elemental composition has 12.6% Na_2O, which was used as a counterion in the simulation.

Figure 1. Descriptive flowchart of the process used to simulate the removal of $Zn^{2+}_{(aq)}$ by NaY zeolite in a fixed bed column, using Aspen Adsorption.

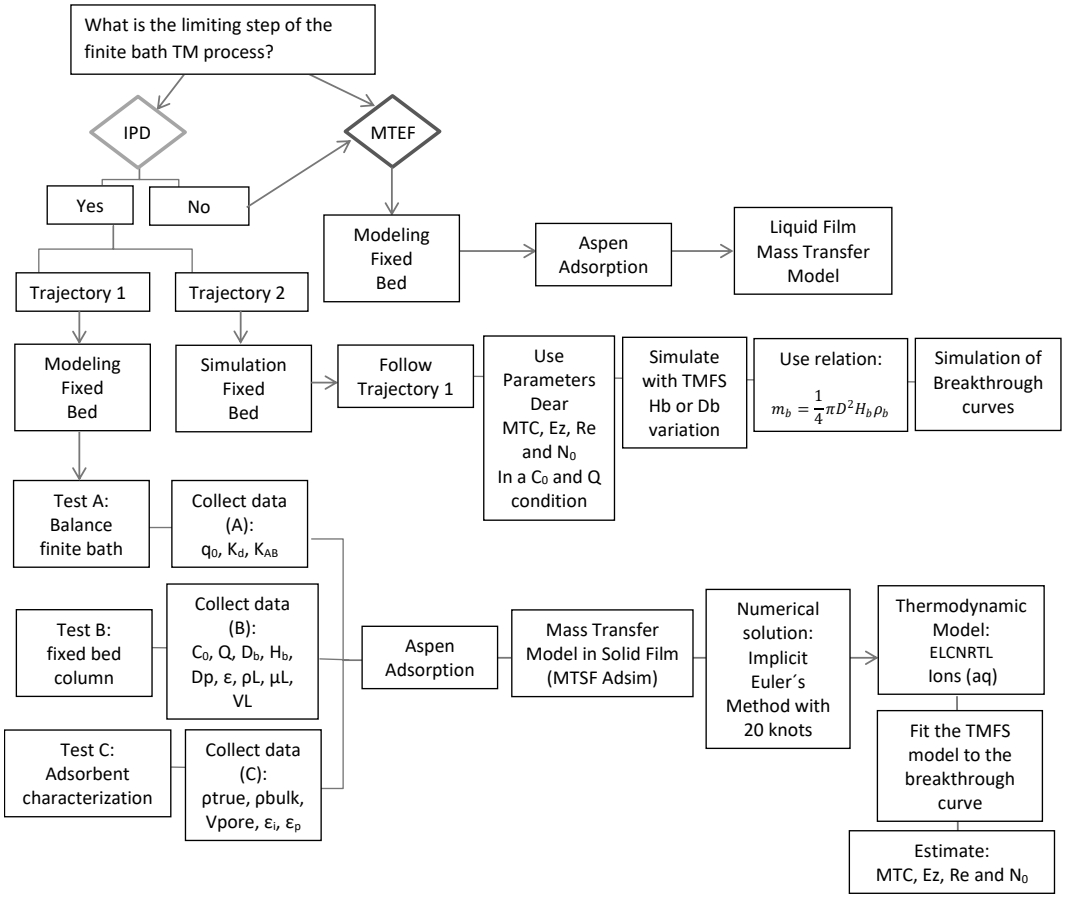

Source: Authors.

It was assumed that the solution was very dilute and that metal ions present in the solution would not significantly affect the density and viscosity of the solution. The density and viscosity of water at 25°C were used, which are respectively 55.41 kmol/m^3 and 8.94×10^{-4} Ns/m^2, as well as molar mass 18.05 kg/kmol.

2.5 Column ion exchange capacity and saturation time

The calculation of ion exchange capacity in fixed bed columns was obtained by mass balance using Equation (18) (Ostroski et al., 2011):

$$q_{eq} = \frac{C_0 Q}{1000 m_s} \int_0^t (1 - C_{out}/C_0)\mathrm{d}t \quad (18)$$

Where q_{eq} is the equilibrium concentration of metal ions in the zeolite (meq/g); m_s is the dry mass of zeolite (g); Q is the volumetric flow rate of the solution (mL/min); t is time in minutes; C_{out} is the cation concentration at the column output (meq/L); C_0 is the cation concentration at the column output (meq/L). Column saturation time was collected when the column reached at least 90% C_0 at the column outlet.

3. Results and Discussion

3.1 Determination of distribution (K_d) and selectivity (K_A^B)

Table 3 shows the estimated coefficients from the isotherms for ion exchange between $Zn^{2+}_{(aq)}$ and NaY zeolite, as well as the statistical evaluation parameters. Observing only the R^2 parameter, it is biased to select the Freundlich and Lambert models as the best fits, to be used in the estimation of K_d.

Table 3. Parameter estimates for fitted linearized empirical models.

Parameter	Model results			
	Linear	**Lambert**	**Freundlich**	**Langmuir**
	$Y = bX$	$Y = bX + cX^2$	$Y = a + bX$	$Y = bX + a$
R^2	0.8448	0.9691	0.9716	0.9064
MSE	0.6498	0.1454	0.0037	0.0048
A	0.0	0.0	0.6769±0.05	0.4084±0.07
B	1.1885±0.38	2.7±0.65	0.3153±0.05	0.0756±0.02
C	n/a	-0.6503±0.26	n/a	n/a
Kd	B=1.1885	B=2.7	Exp.(A)=1.97	1/B=13.2

Source: Authors.

The MSE values are comparable only between the Linear and Lambert models, as the dependent variables are expressed on the same scale, where Lambert had a lower MSE, once again, being the most representative model. Observing the standardized residuals graphs (Figure 2), the Freundlich model showed fit failures characterized by a tendency to overestimate for low equilibrium concentrations, however it presented a residual value within the range of -1.5 to +2.0.

The Lambert model, which resulted in the second highest R^2 and low MSE, showed better random dispersion of the standardized residuals along the X axis, as shown in Figure 2. It was observed that in the Lambert model, the standardized residuals ranged from -1.1541 to 2.0178 while in Freundlich's, they range from -1.1868 to 1.5558.

Regarding the Freundlich model, it is worth remembering that, in this case, the unit of estimated K_d is equal to that of K_f given in $meq.g^{-1}/(meq.L^{-1})$ (Nkedi-Kizza & Brown, 1998). In this model, when the values of the index ($1/n$) of the equation are equal to or close to one, the value of K_f is equivalent to a partition coefficient of the solute between the solution and the solid surface, that is, $K_f = K_d$. However, from the result obtained by the adjustment of $1/n = 0.3153$ shown in Table 3, it was possible to identify that $1/n \neq 1$, therefore $K_f \neq K_d$. Thus, the value estimated by the Lambert model for $K_d = 2.7 \pm 0.65$, with a confidence level of 95%, was chosen to subsequently calculate the coefficient described in item 2.1 using the 3rd equation.

From the results obtained from K_A^B, for tests 1 (0.71), 2 (0.91) and 3 (1.17), with solution concentrations (C_0) equal to 0.844, 0.966 and 1.381 meq/L of $Zn^{2+}_{(aq)}$, respectively, the values of K_A^B presented a growing tendency. According to Bergseth (1980) this behaviour is expected, as the selectivity coefficient increases with the concentration of the external solution and with the content of heavy metal cations bound to the clays.

In tests 4 and 5, the values of K_A^B of 0.76 and 0.93, respectively, with $C_0 = 0.844$ meq/L, presented an increase due to a flow difference of 4 ml/min and 12 ml/min between them, which interfere in q_0 (zeolite ion exchange capacity). The highest value of $K_A^B = 1.17$, referring to test 3 ($C_0 = 1.381$ meq/L and Q=8 mL/min), theoretically characterized the condition of greater resin preference for $Zn^{2+}_{(aq)}$ ion of the external solution. According to Abrão (2014) the higher the selectivity coefficient, the greater the preference of the exchanger material for this ion. The selectivity coefficient had a direct influence

on the modelling of the breakthrough curves; it was one of the data required for the adjustment of the MTSF model in Aspen Adsorption.

Figure 2. Freundlich (a) and Lambert (b) adsorption isotherms models adjusted to data from Ostroski et al. (2008) to obtain K_d and standardized residuals (c) and (d) respectively from the adjustments.

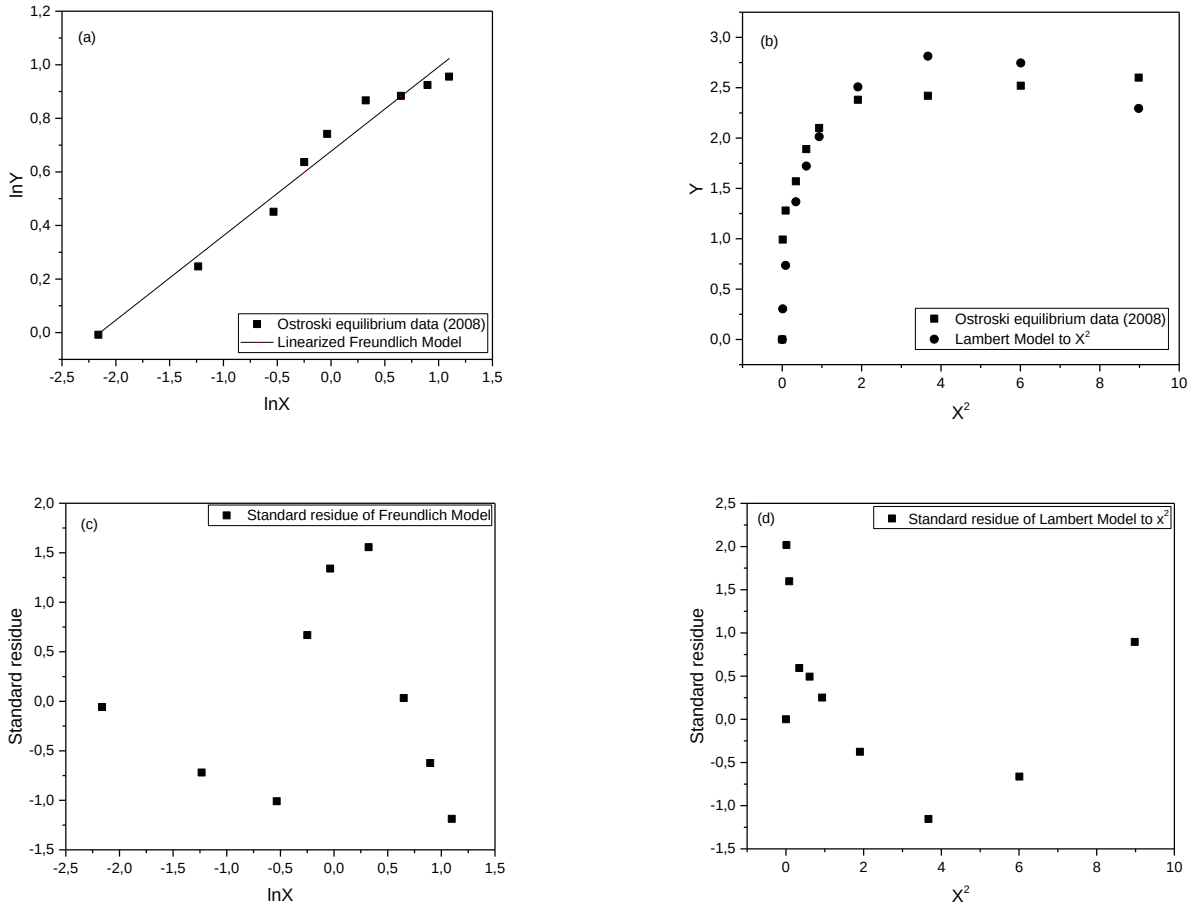

Source: Authors.

3.2 Adjustments of kinetic models from finite bath system

First and second order kinetic models for finite bath data are not able to determine the diffusion mechanisms (Abdi et al., 2017). According to Fagnani et al. (2017) the IPD model identifies the diffusion mechanisms in ion exchange processes with NaY zeolite and represents the ion transport through the zeolite pores. To adjust the IPD and MTEF models, it was necessary to first calculate *q(t)*, with Equation (19) (Ruthven, 1984):

$$q(t) = [C_i - C(t)].\frac{V}{m} \quad (19)$$

Where $q(t)$ is the amount of $Zn^{2+}_{(aq)}$ in the solid phase at time t (meq $Zn^{2+}_{(aq)}$/ g of zeolite NaY); C_i is the initial concentration of $Zn^{2+}_{(aq)}$; $C(t)$ is the concentration of $Zn^{2+}_{(aq)}$ in the liquid phase at time t (meq $Zn^{2+}_{(aq)}$/ L of sol.); V is the volume of 1.5 L of solution and m is the mass of 1g NaY zeolite, obtained from Ostroski et al. (2008).

Thus, when plotting the data of $q(t)$ versus $t^{1/2}$ (minutes$^{0.5}$), it was possible to adjust the IPD model to the kinetic experimental data from Ostroski et al. (2008) and obtain a straight line with slope (I), as highlighted in Figure 3, with a multilinearity indicating more than one limiting step in the process. When this occurs, it can be observed three distinct steps. In the first one, an instantaneous removal of the $Zn^{2+}_{(aq)}$ ions in solution referring to the diffusion in the pores of the external surface of the zeolite; a second stage of gradual removal referring to diffusion into the intraparticle pores; and, finally, a final stage when the ion exchange reaches equilibrium (Chen et al., 2003).

Figure 3. Intraparticle diffusion at a concentration of 2.96 meq.L^{-1}.

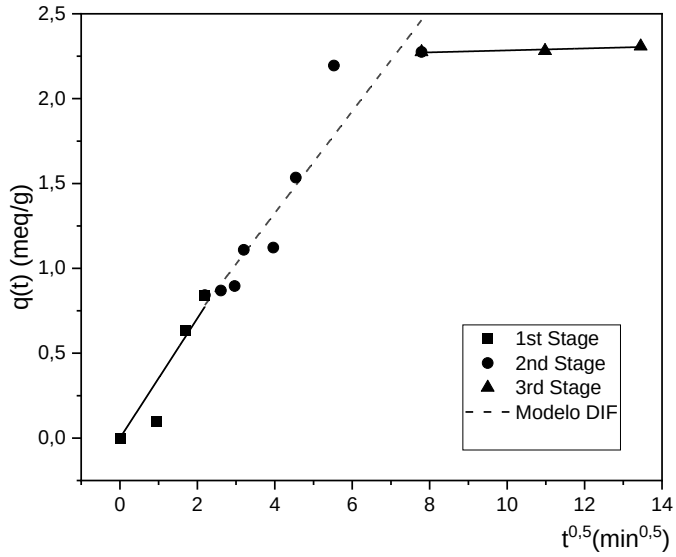

Source: Authors.

Table 4 presents the calculated value for the intraparticle diffusion coefficient (K_p) and the slope (I), through the 2nd stage of the IPD model, with R^2 = 0.89, indicating that intraparticle diffusion also interferes with the speed of the process. Furthermore, it was possible to observe that the value of I was not null, indicating that the boundary layer is representative in the exchange process, as the value of this deviation indicates an approximation of the boundary layer in meq.g^{-1} and thus, the higher this value, the greater its importance to the process. The first stage that obtained a value of R^2 = 0.9099, confirmed that the exchange process is also governed by ion diffusion on the outer surface of the solid (Silva et al., 2015).

The value found for the removal rate of $Zn^{2+}_{(aq)}$ by intraparticle diffusion in the NaY zeolite of $Kp_{Zn(II)}$ = 0.3 meq.g^{-1}.min$^{-0.5}$, was within the intraparticle diffusion capacity of divalent ions of the NaY zeolite found in the literature from 0.105±0.0239 meq.g^{-1}.min$^{-0.5}$ to 0.4968 meq.g^{-1}.min$^{-0.5}$ (Fagnani et al., 2017; Matti & Surchi, 2014).

On the adjustment of the external film mass transfer model (MTEF), when plotting q_t versus t, it was possible to adjust it to the experimental kinetic data of Ostroski et al. (2008) and obtain different curves according to the variation of the initial concentration of $Zn^{2+}_{(aq)}$ in the aqueous medium (C_i), as highlighted in Figure 4.

Table 4. Kinetic adjustment parameters of the ion exchange of $Zn^{2+}_{(aq)}$ and NaY zeolite, using the kinetic curve of Ostroski et al. (2008) and the Intraparticle Diffusion (IPD) model.

C_0 (meq/L)	K_p (meq/g.min$^{0.5}$)	I	IPD (R^2)		
			1st Stage	2nd Stage	3rd Stage
2.96	0.3002	0.12	0.9099	0.8908	0.8508

Source: Authors.

The MTEF fit, a differential model that represents the transport of the ion within the solution to the liquid film layer around the zeolite particles, was performed using the MatLab software, which enabled to simulate the behaviour of MTEF by decreasing the concentration of $Zn^{2+}_{(aq)}$ during ion exchange with NaY zeolite in the finite bath system.

Figure 4. MTEF model and experimental kinetic curve obtained by Ostroski et al. (2008), varying C_0 in $Zn^{2+}_{(aq)}$.

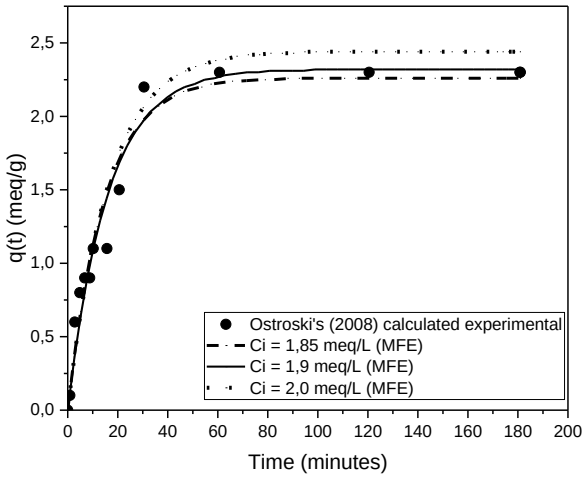

Source: Authors.

As can be seen in Figure 4, the MTEF model presented good adjustment when the *Ci*(*t*) reached the range of 1.85-2.0 meq of $Zn^{2+}_{(aq)}$/L of solution, with the highest $R^2 = 0.8477$, when C_i reaches 1.9 meq of Zn^{2+}/L of solution, as can be seen in table 5. Thus, the mass transfer in the external liquid film is not the limiting step in the zinc removal process by zeolite NaY, since the phenomenon occurred only in a specific range of concentration of the contaminating solution.

Table 5 shows the parameter estimated by the MTEF and the rate of mass transfer rate in the external liquid film (k_{TM}). It was possible to observe that as C_i reduced from 2.0 meq/L to 1.85 meq/L, there was an increase in the k_{TM} value from 0.05 min-1 to 0.0559 min-1, characterizing a decrease in the resistance to mass transfer through the external film to the zeolite NaY (Stephen et al., 2005).

Table 5. Kinetic adjustment parameters of the ion exchange of $Zn^{2+}_{(aq)}$ and NaY zeolite

Model	Parameter	C_i (meq/L)		
		2.0	**1.9**	**1.85**
MTEF	K_{TM} (min-1)	0.0500	0.0501	0.0559
	R^2	0.8313	0.8477	0.8348
	Standard Error	$1.60x10^{-9}$	$3.58x10^{-11}$	$1.22x10^{-10}$

Source: Authors.

In general, both MTEF and IPD mass transfer processes are present in the ion exchange process, however, the limiting step was the intraparticle diffusion (IPD), with better fits, which was expected since, according to Ruthven (1984), pelletized materials, such as NaY zeolite from Ostroski et al. (2008), show resistance to diffusion in their micro and macropores.

From this pre-definition, it was possible to later choose the most representative model for the modelling and simulation of a fixed bed column in Aspen Adsorption, since the software has two options for ion exchange processes, fluid film model (limited by the MTEF phenomenon) and solid film model (limited by the IPD phenomenon). Thus, the previous study of finite bath kinetics allowed to define that the solid film mass transfer model (MTSF) is the most representative for the process.

3.3 Breakthrough curves and calculated parameters of MTSF, TH and YN models

At this stage of the research, the breakthrough curves obtained by Ostroski et al. (2008) were modelled for $Zn^{2+}_{(aq)}$ removal in a column filled with NaY zeolite, using solid film mass transfer models (MTSF), Thomas (TH) and of Yoon-Nelson (YN), in order to define the most representative model for the process. The parameters estimated by adjusting the models to the breakthrough curves are listed in Table 6 and each one of them allowed different considerations.

Table 6. Parameters estimated by the different models obtained from the adjustment to the data from Ostroski et al. (2008) experimental breakthrough curves

Model	Parameters	C_0[a]			Q[b]		
		0.844 meq/L	**0.966 meq/L**	**1,381 meq/L**	**4 mL/min**	**8 mL/min**	**12 mL/min**
Aspen Adsorption (MTSF)	MTC (min^{-1})	0.02598	0.01505	0.0209	0.0081	0.0251	0.0246
	Ez (m^2/s)	1.62x10-6	1.63x10-6	1.63x10-6	8.13x10-7	1.62x10-6	2.44x10-6
	Re	0.8411	0.8439	0.8439	0.4221	0.8419	1.2661
	N_0 (eq/m^3)	1,990.45	1,832.25	1,916.51	1,870.0	1,990.45	1711.26
	R^2	0.9977	0.9923	0.9947	0.9970	0.9977	0.9955
Thomas (TH)	KTH (L/meq.min)	0.06	0.034	0.033	0.022	0.06	0.061
	q_0 (meq/g)	2.33	2.09	2.14	2.13	2.33	1.91
	R^2	0.9985	0.9972	0.9683	0.9793	0.9985	0.9873
Yoon - Nelson (YN)	K_{YN} (min^{-1})	0.0507	0.033	0.0458	0.0186	0.0507	0.0516
	τ (min)	272.9	215.18	162.23	495.70	272.9	147.81
	R^2	0.9985	0.9972	0.9683	0.9793	0.9985	0.9873

a) Flow (Q): 8 ml/min; Column height (Hb): 0.03 m; b) Feed concentration (C0): 0.844 meq/L; Column height (Hb): 0.03 m.

Source: Authors.

On the Thomas model, it was possible to observe that the velocity constant (K_{TH}) decreased as the feed concentration (C_0) increased and increased as the flow (Q) increased. Zheng et al. (2008) and Trgo et al. (2011) obtained similar behaviours when evaluating the ion exchange in zeolites. The highest zinc removal capacity by the NaY zeolite bed, estimated by the Thomas model, was q_0 = 2.33 meq/g under lower C_0 and reduced as the flow increased. The TH model, which disregards axial dispersions in the bed, presented R^2 = 0.9683 to 0.9985, while the MTSF model that considers them stood out as being able to predict the curve advance with R^2 = 0.9923 to 0.9977, as C_0 and Q varied.

In the MTSF model of Aspen Adsorption, which considers the presence of axial dispersion in the hydrodynamic conditions of the column, as can be seen in Table 6, it resulted in E_z values sensitive to flow variation. As Q increased, E_z increased since their estimates are linked to the velocity of the fluid flow, which also increases as flow increases. This same behaviour for E_z was found by Abdi and Abedini (2020) when estimating it in a fixed bed column using Aspen Adsorption. The Reynolds numbers of the process, regardless the variation of Q, resulted in Re < 1.3 and according to Slater (1991) for fixed bed columns, a Re < 2 characterizes a non-turbulent liquid flow. Vermeulen (1958) suggests that the axial mixture can be neglected if Re > 0.1 under V_L = 0.00014 m/s, however the liquid velocity reached values of 0.001048, 0.002091 and 0.003144 m/s for Q = 4, 8 and 12 mL/min, respectively, that is, the axial dispersion was significant for the column that is not operating under a plug flow condition. Figure 5 shows the breakthrough curves for each model.

Figure 5. TH, YH and MTSF models, adjusted to the experimental breakthrough curves of Ostroski et al. (2008) by varying the feed flow at 0.844 meq/L: (a) 4 mL/min, (b) 8 mL/min and (c) 12 mL/min, and, by varying the feed concentration at 8 mL/min: (d) C_0 = 0.966 meq/L and (e) C_0 = 1.381 meq/L.

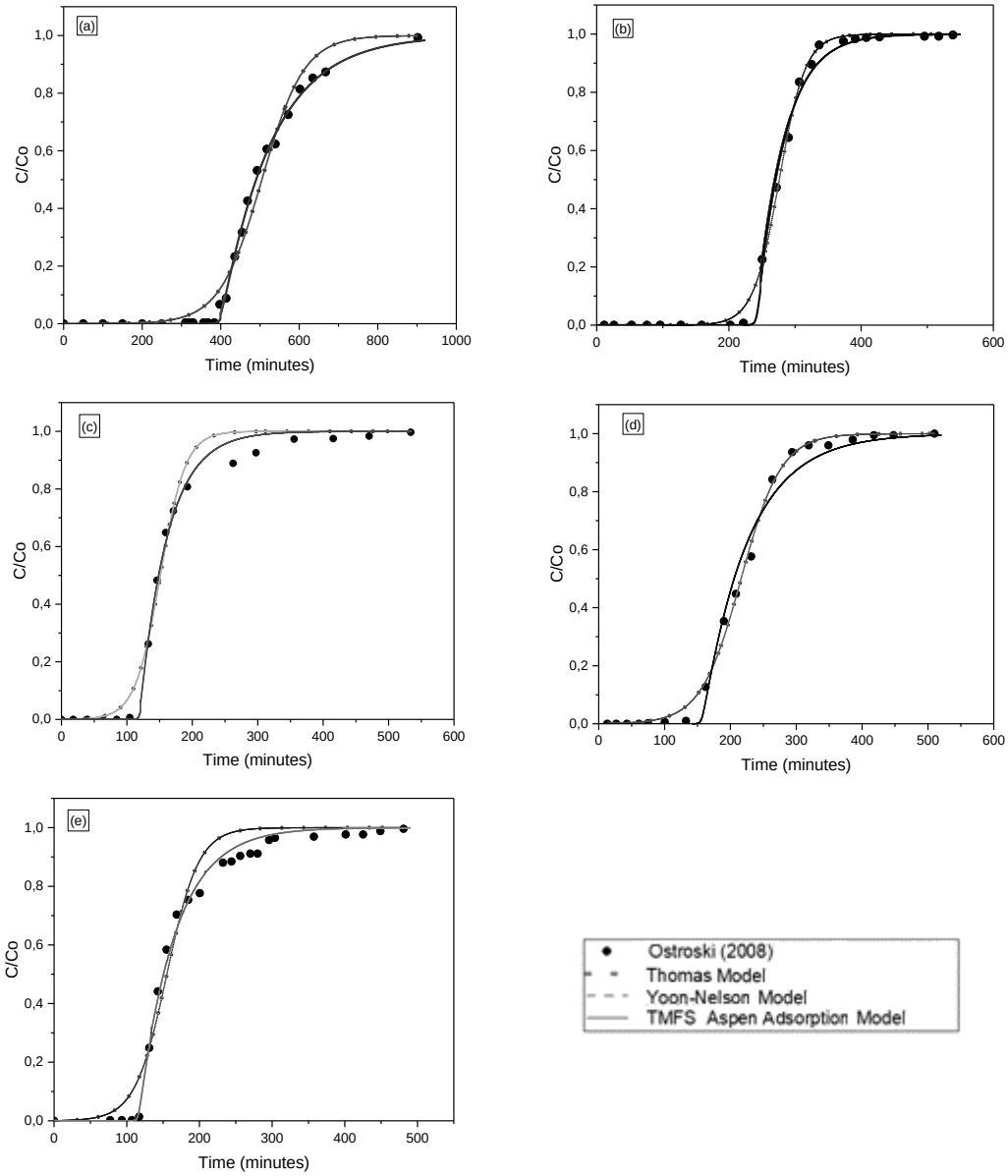

Source: Authors.

According to Figure 5(c), a flatter breakthrough curve front and earlier rupture point were observed compared to Figures 5(a) and 5(b) with the same C_0. Observing data in Table 6 for Figure 5(c), the MTSF model estimated the lowest volumetric capacity for removing $Zn^{2+}_{(aq)}$ by zeolite NaY (N_0 = 1,711.26 eq/m^3), under the operating conditions of higher flow (Q = 12 mL/min), higher axial dispersion (E_z = 2.44x10-6 m^2/s), higher Reynolds number (Re = 1.2661) and one of the highest mass transfer coefficients (MTC = 0.0246339 min^{-1}), under C_0 = 0.844 meq/L. Thus, the increase in flow raised the values of MTC and E_z, resulting in an increase in the speed of ion exchange and bed saturation.

The Yoon-Nelson model presented relative approximation under the estimated saturation point where $C/C_0 = 0.5.C_0$ and the experimental. Figures (a), (b), (c), (d) and (e) presented τ(min) = 495.7; 272.9; 147.81; 215.18 and 162.23 for model YN, respectively, while Ostroski et al. (2008) obtained τ(min) = 492.84; 271.96; 146.1; 208.4 and 142.7. Furthermore, τ

decreased when increasing C_0 and Q. Yoon-Nelson's removal rate constant of $Zn^{2+}_{(aq)}$, K_{YN} (min^{-1}), consequently increased when increasing C_0 and Q. This behaviour is similar to that found in the literature for application of this model in adsorption with zeolites (Trgo et al., 2011). However, the Yoon-Nelson model resulted in R^2 between 0.9683 and 0.9985, varying in relation to changes in C_0 and Q.

Therefore, given the above discussions, the greater significance of using the MTSF model of Aspen Adsorption to simulate the ion exchange process in the removal of Zn^{2+}(aq) by zeolite NaY was validated, as it could predict the experimental data with good accuracy and, regardless of the variation of the C_0 and Q.

3.4 Simulation of Breakthrough Curves

Figure 6 shows the flowchart implemented in the Aspen Adsorption environment to simulate the breakthrough curves. The necessary input data that were used for simulation using the MTSF model, of the ion exchange between $Zn^{2+}_{(aq)}$ and zeolite NaY, were MTC = 0.0259854 min^{-1}, E_z = 1.62x10^{-6} m^2/s and N_0 = 1990.45 eq/m^3.

Figure 6. Flowchart of fixed bed column implemented in Aspen Adsorption.

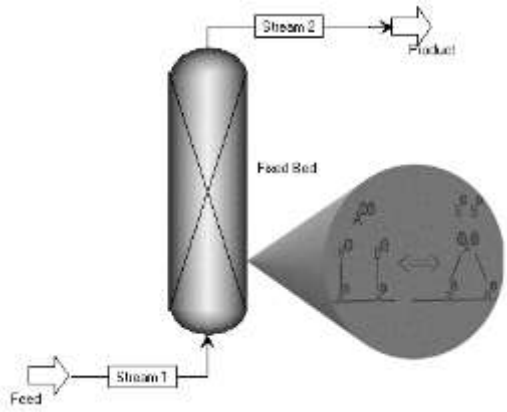

Source: Authors.

The operating conditions used to estimate them were C_0 = 0.844 meq/L, Q = 8 mL/min, D_b = 0.009 m, ε_i = 0.5 m^3/m^3, ε_p = 5.99x10^{-4} m^3/m^3, IP1(K_A^B) = 0.7, IP2 (ionic charge) = 2+, ρ_b= 420000 g/cm^3. Only the height (Hb) of the column was changed. Figure 7 shows the breakthrough curves generated with Aspen Adsorption, with height of the fixed bed of 0.012, 0.015, 0.03, 0.06 and 0.08 meters, respectively.

The results of the breakthrough curves show that as the bed height increased, the breakthrough moment increased. Thus, there was a greater efficiency in removing $Zn^{2+}_{(aq)}$, since the zinc ions had greater contact with the NaY zeolite, as expected. A higher column has greater available surface area, which provides more active site for ion exchange, resulting in an increase in time to reach breakthrough point. Thus, a greater removal of metal is observed.

In quantitative terms, Table 7 compares the experimental ion exchange capacity from Ostroski et al. (2008) with q_0 = 2.36 meq/g, and calculated with Equation (18) under the curves estimated with the MTSF Adsim model with q_0 = 2.38 meq/g, demonstrating the good fit of the model. The proximity of estimated q_0 with the experimental q_0, both for H_b= 0.03 m, as well as presenting q_0 calculated for the simulated curves with variations of H_{bs} = 0.012, 0.015, 0.06 and 0.08 meters (m).

Figure 7. Comparison of breakthrough curves for constant flow rate, constant initial concentration and variable bed height.

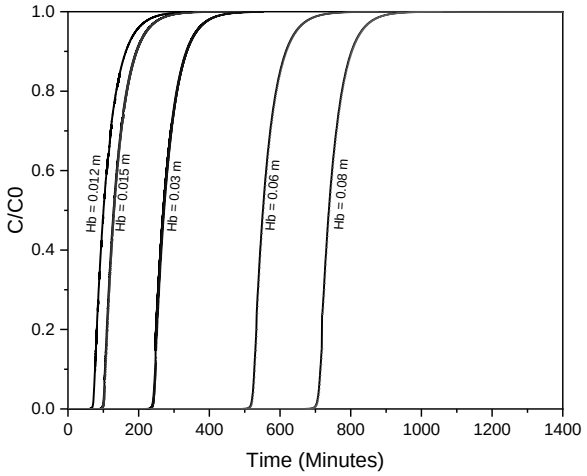

Source: Authors.

Table 7. Comparison of the influence of the variation in column height and fixed bed.

Parameters	H_{be}[(a)](m)	H_{bm}[(b)] (m)	H_{bs} [(c)] (m)			
	0.03	**0.03**	**0.012**	**0.015**	**0.06**	**0.08**
q_0 (meq/g)	2.36	2.38	0.95	1.19	4.77	6.33
t (min)	336.0	332.8	282	311	693	876
m (g)	0.8	0.8	0.31	0.4	1.6	2.13

[(a)]Exp. from Ostroski et al. (2008) [(b)]Modelled with Adsim; [(c)]Simulated with Adsim.

Source: Authors.

Analyzing data from Table 7, it was noticed that q_0 gradually increased with the increase in height and mass of NaY zeolite, as expected. The authors Nieva et al. (2019) and Adornado et al. (2016) found similar behaviours with the variation of Hb, for the estimated breakthrough curves for ion exchange of metallic ions with biomass, using the MTSF model of Adsim. A column with lower height implies a lower capacity of the bed to remove metal ions from the solution and, therefore, resulting in a faster rupture and saturation time, as shown in Table 7, where the shortest saturation time (t = 282 min) was detected for the lowest height (Hb = 0.012 m). Also, at lower bed heights, axial dispersion is considered as the predominant mass transfer phenomenon that reduces the diffusion of metallic ions (Singha et al., 2012).

4. Conclusion

The kinetic modelling with finite bath data allowed to stablish that the limiting step of the exchange process, between the IPD and MTEF models, is the intraparticle diffusion, with $R^2 = 0.9099$ for the 1st stage of instantaneous ion exchange between $Zn^{2+}_{(aq)}$ and the surface of zeolite NaY, and $R^2 = 0.8908$ for the 2nd stage of gradual ion exchange within the pores of the zeolite. The kinetic modelling of fixed bed column using the MTSF, TH and YN models demonstrated that the Adsim MTSF model, which also considers intraparticle diffusion as one of the limiting phenomena, presented the best fit ($R^2 \geq 0.9923$). TH and YN resulted in $R^2 \geq 0.9683$. The mass transfer (MTC) and axial dispersion (E_z) phenomena identified by the Adsim MTSF model demonstrated that N_0 and t, from the NaY zeolite bed, increased as the values of MTC and E_z decreased, as well as N_0 and t decreased as MTC and E_z increased. The increase of C_0 and Q resulted in high MTC and E_z. Due to the bed's sensitivity to these phenomena, the importance of including these terms in the mass balances became evident, but only for values of C_0 and Q studied in this work. Based on the results of the simulation, it was noticed that the increase in H_b

increases q_0 and t. For lower H_b values, the axial dispersion was considered as the predominant mass transfer phenomenon, thus reducing the diffusion of $Zn^{2+}_{(aq)}$ metallic ions. It can be concluded that a multi-scale treatment system design for the removal of $Zn^{2+}_{(aq)}$ ions from wastewater streams using a fixed bed column filled with NaY zeolite can be achieved using the validated model obtained in Aspen Adsorption.

Acknowledgments

The authors thank the Coordenação de Aperfeiçoamento de Pessoal de Nível Superior (CAPES) for financial support for this work.

References

Abdi, J., & Abedini, H. (2020). MOF-based polymeric nanocomposite beads as an efficient adsorbent for wastewater treatment in batch and continuous systems: Modelling and experiment. *Chemical Engineering Journal*, 400.

Abdi, J., Vossoughi, M., Mahmoodi, N. M., & Alemzadeh, I. (2017). Synthesis of metal-organic framework hybrid nanocomposites based on GO and CNT with high adsorption capacity for dye removal. *Chemical Engineering Journal*, 326, 1145–1158.

Abrão, A. (2014). Operações de troca iônica. IPEN.

Adornado, A. P., Soriano, A. B., Orfiana, O. N., Pangon, M. B. J., & Nieva, A. D. (2016). Simulated biosorption of cd(ii) and cu(ii) in single and binary metal systems by water hyacinth (eichhornia crassipes) using aspen adsorption. *Asean Journal of Chemical Engineering*, 16(2), 21–43.

Bergseth, H. (1980). Selektivität von IIIit, Vermiculit und Smectit gegenüber Cu2+, Pb2+, Zn2+, Cd2+ und Mn2+. *Acta Agriculturae Scandinavica*, 30(4), 460–468.

Calábria, J. A. A., Ladeira, A. C. Q., & Cota, S. D. S. (2017). Estudo da sorção de césio em solos: Avaliação do desempenho em repositório de rejeitos radioativos. *Revista Ibero-Americana de Ciências Ambientais*, 8(2), 190–204.

Calvet, R. (1989). Adsorption of organic chemicals in soils. *Environmental Health Perspectives*, 83, 145–177.

Chen, J. P., Wu, S., & Chong, K. H. (2003). Surface modification of a granular activated carbon by citric acid for enhancement of copper adsorption. *Carbon*, 41, 1979–1986.

Cupertino, M. C., Moreira, I. F. V., Coelho, M. A., Amaral, Y. F. Q., & Teixeira, D. C. L. (2020). Exposição a contaminantes ambientais inorgânicos e danos à saúde humana. *Brazilian Journal of Health Review*, 3(4), 10353–10369.

Fagnani, H. M. C., Deolin, M. E., Clays, M. A. D., & Arroyo, P. A. (2017). Identificação dos mecanismos de sorção em zeólita NaY e sílica gel. *Revista Matéria*, 22(3).

Jung, K. W., Jeong, T. U., Choi, J. W., Ahn, K. H., & Lee, S. H. (2017). Adsorption of phosphate from aqueous solution using electrochemically modified biochar calcium-alginate beads: Batch and fixed-bed column performance. *Bioresource Technology*, 244, 23–32.

Lambert, S. M. (1967). Functional relationship between sorption in soil and chemical structure. *J. Agr. Food Chem.*, 15(4), 572–576.

Lattanzi, A. M., Pecha, M. B., Bharadwaj, V. S., & Ciesielski, P. N. (2020). Beyond the effectiveness factor: Multi-step reactions with intraparticle diffusion limitations. *Chemical Engineering Journal*, 380.

Lazzaretti, L. L., & Hupffer, H. M. (2018). Nanotecnologia: O olhar da ciência sobre a toxicidade e os potenciais riscos desses produtos. *Revista Conhecimento Online*, 3(10), 79–100.

Matti, A. H., & Surchi, K. M. (2014). Kinetics of cation exchange capacity of homoionic sodium form nay zeolite. International Journal of Innovative Research in Science, *Engineering and Technology*, 3(6), 13137–13145.

Montgomery, O. C., & Peck, E. A. (1982). Introduction to linear regression analysis. John Wiley & Sons.

Nakajima, H. (2013). Mass transfer: Advances in sustainable energy and environment oriented numerical modelling. IntechOpen.

Nieva, A. D., Andres, J. C. S., & Gonzales, K. P. (2018). Simulated biosorption of cu2+ in aqueous solutions using cucumis melo VAR. cantalupensis. IOP Conf. Series: *Earth and Environmental Science*, 191.

Nieva, A. D., Garcia, R. C., & Ped, R. M. R. (2019). Simulated biosorption of cr6+ using peels of litchi chinensis sonn by aspen adsorption® V8.4. *International Journal of Environmental Science and Development*, 10(10), 331–337.

Nkedi-Kizza, P., & Brown, K. D. (1998). Sorption, degradation and mineralization of carbaryl in soils , for single-pesticide and multiple-pesticide systems. *Journal Environmental Quality*, 27, 1318–1324.

Oliveira, G. M. T. S., Oliveira, E. S., Santos, M. L. S., Melo, N. F. A. C., & Krag, M. N. (2018). Concentrações de metais pesados nos sedimentos do lago água preta (pará, brasil). *Engenharia Sanitária e Ambiental*, 23(3), 599–605.

Ostroski, I. C., Barros, M. A. S. D., Silva, E. A., Dantas, J. H., Arroyo, P. A., & Lima, O. C. M. (2008). A comparative study for the ion exchange of Fe(III) and Zn(II) on zeolite NaY. *Journal of Hazardous Materials*, 161, 1404–1412.

Ostroski, I. C., Dantas, J. H., Canavesi, R. L. S., Silva, E. A., Arroyo, P. A., & Barros, M. A. S. D. (2011). Removal of Fe (II) in fixed bed of NaY zeolite. *Acta Scientiarum Technology*, 33(3), 305–312.

Puranik, P. R., Modak, J. M., & Paknikar, K. M. (1999). A comparative study of the mass transfer kinetics of metal biosorption by microbial biomass. *Hydrometallurgy*, 52, 189–197.

Ruthven, D. M. (1984). Principles of adsorption and adsorption processes. Wiley and Sons.

Silva, M. A., & Miranda, M. N. N. (2003). Estimation of properties of ternary mixtures of solids using the mixing rule. Powder *Technology*, 134, 16–23.

Silva, M. A., & Souza, F. V. (2004). Drying behavior of binary mixtures of solids. *Drying Technology: An International Journal*, 22, 165–177.

Silva, R. T. S., Dervanoski, A., Haupenthal, L. D., Souza, S. M. A. G. U., Souza, A. A. U., & Luz, C. (2015). Simulação numérica e ensaios experimentais da remoção de Fe (III) da água para utilização nas indústrias alimentícias. *Engenharia Sanitária Ambiental*, 20(4), 653–663.

Singha, S., Sarkar, U., Mondal, S., & Saha, S. (2012). Transient behavior of a packed column of Eichhornia crassipes stem for the removal of hexavalent chromium. *Desalination*, 297, 48–58.

Slater, M. J. (1991). The principles of ion exchange technology. Butterworth-Heinemann.

Souza, M. D., Boeira, R. C., Gomes, M. A. F., Ferracini, V. L., & Maia, A. H. N. (2001). Adsorção e lixiviação de tebuthiuron em três tipos de solo. R*evista Brasileira de Ciências do Solo*, 25, 1053–1061.

Stephen, J. A., Gan, Q., Matthews, R., & Johnson, A. (2005). Mass transfer processes in the adsorption of basic dyes by peanut hulls. Industrial Engineering *Chemical Research*, 44, 1942–1949.

Tantet, J., Eic, M., & Desai, R. (1994). Experimental and theoretical studies of sulfur dioxide and water adsorption in hydrophobic zeolites. Studies in Surface *Science and Catalysis*, 84, 1269–1276.

Thomas, H. C. (1944). Heterogeneous ion exchange in a flowing system. *Journal of the American Chemical Society*, 66, 1664–1666.

Trgo, M., Medvidovic, N. V., & Perié, J. (2011). Application of mathematical empirical models to dynamic removal of lead on natural zeolite clinoptilolite in a fixed bed column. *Indian Journal of Chemical Technology*, 18, 123–131.

Vermeulen, T. (1958). Advances in chemical engineering. Academic Press.

Zhang, Y. P., Adi, V. S. K., Huang, H. L., Lin, H. P., & Huang, Z. H. (2019). Adsorption of metal ions with biochars derived from biomass wastes in a fixed column: Adsorption isotherm and process simulation. *Journal of Industrial and Engineering Chemistry*, 76, 240–244.

Zheng, H., Han, L., Ma, H., Zheng, Y., Zhang, H., Liu, D., & Liang, S. (2008). Adsorption characteristics of ammonium ion by zeolite 13X. *Journal of Hazardous Materials*, 158, 577–584.